A Coupled-Inductor-Based Buck–Boost AC–DC Converter With Balanced DC Output Voltages

Wang, Houqing; Wu, Weimin; Li, YunWei; Blaabjerg, Frede

Published in:
I E E E Transactions on Power Electronics

DOI (link to publication from Publisher):
10.1109/TPEL.2018.2820173

Publication date:
2019

Document Version
Accepted author manuscript, peer reviewed version

This article has been accepted for publication in a future issue of this journal, but has not been fully edited. Content may change prior to final publication. Citation information: DOI 10.1109/TPEL.2018.2820173, IEEE Transactions on Power Electronics

A Coupled-Inductor-Based Buck-Boost AC/DC Converter with Balanced DC Output Voltages

Houqing Wang, Weimin Wu, Yunwei Li, *Senior Member, IEEE*, Frede Blaabjerg, *Fellow, IEEE*

***Abstract*—With the development of distributed power generation sources and the widely used DC characterized loads, the DC Nano-grid becomes more and more attractive and the converters with three terminal outputs are increasingly studied. Considering the costs, the efficiency and also the safety, the grounding configuration needs to be addressed when designing the AC/DC converter for a DC Nano-grid system. An AC/DC converter with three terminal outputs has been presented for the united grounding configuration based DC Nano-grid. Nevertheless, for this type of converters, the output voltages are unbalanced in case of unequal DC loads. This paper proposes a novel Buck-Boost AC/DC converter with the capacity of output voltages self-balancing by using a coupled inductor. The operation of this converter will be presented in details through analyzing its equivalent circuits. The small signal model of system in different working modes is given, and the whole system control diagram shows how to balance the DC output voltages. A 220 V/50 Hz/1.5 kW prototype has been developed. Experiments are carried out to verify the effectiveness of the coupled-inductor-based converter.**

***Keywords*—Voltage Balancing, DC Nano-grid, AC/DC Converter, Coupled Inductor, Buck-Boost**

Authors :

1. Houqing Wang
2. Weimin Wu
3. Yunwei Li
4 Frede Blaabjerg

Address:

1, 2 Research Institute of Electronic Automation
Shanghai Maritime University
Shanghai 201306, China

3 Department of Electrical and Computer Engineering
11-370 Donadeo Innovation Centre for Engineering
9211-116 Sreet NW
Edmonton, AB, T6G 1H9, Canada

4 Department of Energy Technology
Pontoppidanstræde 101
Room: 76
9220 Aalborg Ø, DK

Email:

1. houqingok@163.com
2. wmwu@shmtu.edu.cn
3. yunwei.li@ualberta.ca
4. fbl@et.aau.dk

Corresponding Author: Weimin Wu

This article has been accepted for publication in a future issue of this journal, but has not been fully edited. Content may change prior to final publication. Citation information: DOI 10.1109/TPEL.2018.2820173, IEEE Transactions on Power Electronics

I. INTRODUCTION

Due to the energy crisis and the environmental pollution caused by the consumption of fossil fuel, the development of renewable energy generation has been an increasingly critical topic [1]-[4]. Since renewable energies have the intrinsic intermittence and fluctuation, in order to improve the reliability and the quality of power supply, Nano-grids [3], [5], [6] have been proposed to facilitate the connection of renewable power sources to the traditional AC power system. On the one hand, now most renewable power conversion systems are connected into AC Nano-grids [7]. On the other hand, more and more loads show DC characteristics [6], [8]-[11], for example, the variable frequency drives, the LED lighting applications, the computer power supplies and the data centers [10], [11], which constitute a significant portion of the energy consuming loads [8]. If the renewable energies can be directly utilized via the DC Nano-grids, the total energy efficiency will be obviously improved. Therefore, the researches on the DC Nano-grids are drawing more and more attention [8]-[20], especially for the control of AC/DC topologies [12], [15]-[19], which interface with the DC Nano-grid and the traditional AC power systems.

In order to flexibly utilize the DC power generated by the renewable energy sources, a bi-directional AC/DC converter is generally applied to the connection between the DC Nano-grid and the AC power system. However, in some areas, due to the high population density, the renewable powers generally cannot meet the power demand of local loads, so the connection can be simplified into a power factor correction circuit. It should be pointed out, when designing the AC/DC converter for a DC Nano-grid, the grounding configuration needs to be addressed [20], since it determines the costs, the efficiency and also the safety of DC Nano-grid system. In [21]-[25], different AC/DC converters were reviewed and compared, but the suitable AC/DC converters for the united grounding-configuration-based DC Nano-grid application were not introduced. Thus, as shown in Fig. 1, a high efficiency and low cost dual Buck-Boost AC/DC converter with three terminal outputs for DC Nano-grid was proposed in [26], which can use the same ground line to connect the AC system with the DC system, without any insulating transformer. Nevertheless, when the two output loads become unequal, the two output voltages of the conventional converter would be unbalanced.

Various voltage balancing methods have been proposed in [27]-[32]. However, these methods, such as the space vector PWM (SVPWM) [27], [28], the predictive control strategy [29], [30], and the auxiliary balancing circuits [31], [32], are applied to realize the DC link capacitor voltage balance in multilevel multiphase converters, and not suitable for the single phase topology as introduced in [26]. This paper proposes a novel Buck-Boost AC/DC converter with the capability of output voltage self-balancing by using a coupled inductor, where the smaller size and the lighter weight of magnetic material can be achieved [33], compared with the conventional dual Buck-Boost AC/DC converter in [26].

The rest of this paper is organized as follows. The conventional dual Buck-Boost AC/DC converter in [26] and its operating principle are first briefly introduced in section II. In section III, the coupled-inductor-based converter is proposed and its

This article has been accepted for publication in a future issue of this journal, but has not been fully edited. Content may change prior to final publication. Citation information: DOI 10.1109/TPEL.2018.2820173, IEEE Transactions on Power Electronics

operating principle is illustrated via the equivalent circuits in the different working states. In section IV, the modeling is given using the small signal model method and the control diagram is derived. The experimental results are presented in section V to verify the theoretical analysis as well as the principle of operation. Finally, the conclusions are drawn in Section VI.

II. CONVENTIONAL dual BUCK-BOOST AC/DC CONVERTER

Fig. 1 shows the configuration of conventional dual Buck-Boost AC/DC converter for DC Nano-grid with three terminal outputs [26]. R_1 and R_2 are the load resistors. In order to achieve high efficiency, MOSFET devices are adopted and only one switch of this converter is chopping at high frequency at any time. Dependent on the amplitude relation between the output DC voltage (E_1, E_2) and the grid voltage (V_g), the working modes of the conventional dual Buck-Boost AC/DC converter can be divided into the pure boost mode and the buck-boost mode as shown in Fig. 2. During the positive period of the AC voltage, the devices in red work while the devices in blue are off. During the negative period of the AC voltage, the devices in blue work while the devices in red are off.

Note that when the two output DC loads become unequal, for example, due to the connection of different household appliances, the two output voltages would be unbalanced, which limits the application area of this converter. Thus, in order to enable the output DC voltages to be balanced, some extra measures should be taken.

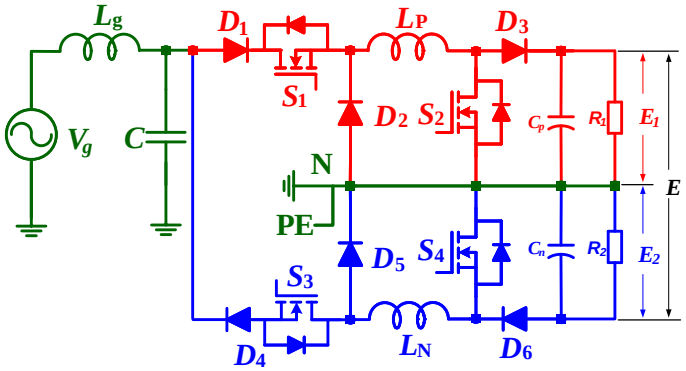

Fig. 1. Conventional dual Buck-Boost AC/DC converter with three terminal outputs proposed in [26].

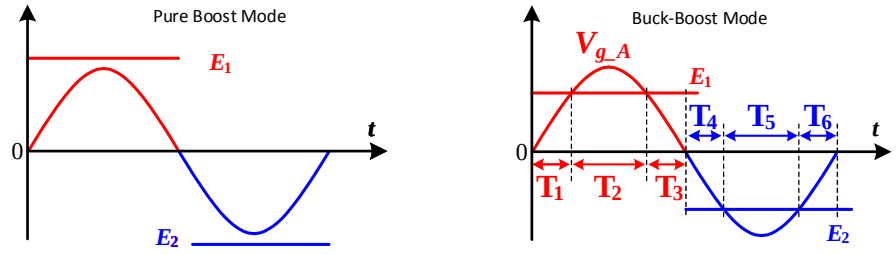

(a) (b)

Fig. 2. Operating modes of Conventional dual Buck-Boost AC/DC converter (a) when $|E_1|$ and $|E_2| > V_{g\_A}$. (b) when $|E_1|$ and $|E_2| < V_{g\_A}$.

III. PROPOSED BUCK-BOOST AC/DC CONVERTER WITH BALANCED DC OUTPUT VOLTAGES

A. Proposed Topology

This article has been accepted for publication in a future issue of this journal, but has not been fully edited. Content may change prior to final publication. Citation information: DOI 10.1109/TPEL.2018.2820173, IEEE Transactions on Power Electronics

Fig. 3 shows two kinds of proposed AC/DC converters as the interface between the DC Nano-grid with three terminals and the low voltage AC power system. Just like the converter presented in [26], the proposed converter also has a vertical symmetrical structure without any insulating transformer, where the main difference involves the coupled DC inductor with two winds (L_P and L_N) and two additional switches (S_5 and S_6). Compared with the converter shown in Fig. 3 (a), S_5 and S_6 of Fig. 3 (b) do not locate in the main power loop, resulting in less power losses. So, in this paper, the topology in Fig. 3 (b) is chosen for the following analysis.

Using the principle of a transformer, the coupled inductor shown in Fig. 3 can transfer the energy of AC source to the positive (or negative) DC output as required. The turns of primary and secondary side windings of coupled inductor are equal. In order to improve the efficiency of energy transfer, the windings must be tightly coupled to ensure a very small leakage inductance inherent in each winding. This can be done by following the winding style used in [34].

As shown in Fig. 3 (b), when R_1 is larger than R_2, in order to balance the output DC voltages, the AC source should supply partial power towards R_2 during the positive period of the AC voltage. Similarly, if R_1 is smaller than R_2, the AC source should provide partial power towards R_1 during the negative period of the AC voltage. In this paper, it is assumed that R_1 is larger than R_2.

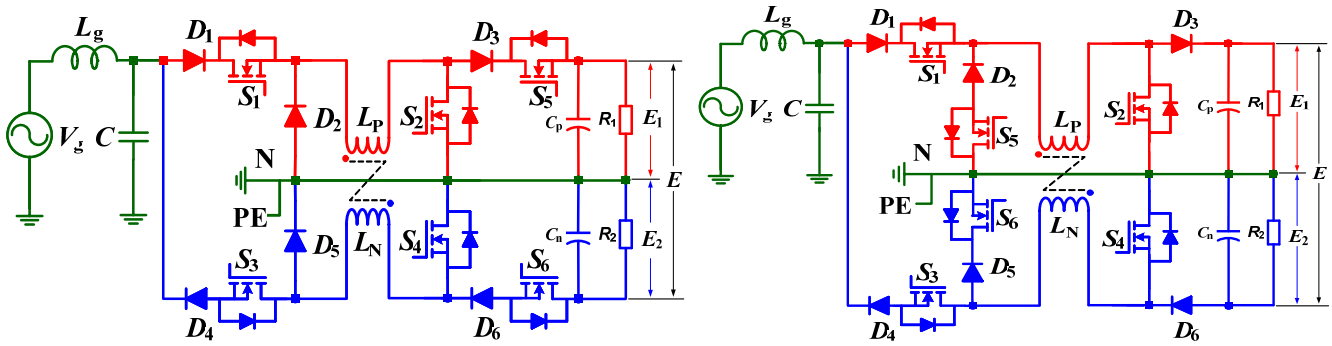

Fig. 3. Proposed AC/DC converter with the capacity of DC output voltages self-balancing.
(a)S_5, S_6 are in main power loop. (b) S_5, S_6 are in freewheeling loop.

B. Operating Modes and Principle of Proposed AC/DC Converter

Similar to the conventional dual Buck-Boost AC/DC converter for DC Nano-grid with three terminal outputs, the working modes of proposed converter are also dependent on the amplitude relation between the output DC voltage (E_1, E_2) and the grid voltage (V_g) as shown in Fig. 2. When $|E_1|$ and $|E_2| \geqslant V_{g\_A}$, there are only two working states in a line period of AC voltage, while when $|E_1|$ and $|E_2| < V_{g\_A}$, there are six working states in a line period. Note that for the proposed AC/DC converter, the voltage difference between the two output DC voltages also determines the exact working state. For the convenience of analysis, ε_1 is defined as the maximum tolerant difference between two output DC voltages. ε_2 is defined as the regulation threshold difference between two output DC voltages, where when $|E_1|-|E_2|> \varepsilon_2$, the output DC voltages need

This article has been accepted for publication in a future issue of this journal, but has not been fully edited. Content may change prior to final publication. Citation information: DOI 10.1109/TPEL.2018.2820173, IEEE Transactions on Power Electronics

to be regulated. Generally, ε_1 is larger than ε_2. Thus, the operating modes of proposed AC/DC converter can be decomposed as following:

1) $|E_1|$ or $|E_2| \geq V_{g\_A}$

When $|E_1|-|E_2|< \varepsilon_2$, the equivalent circuits are shown in Fig. 4, where the system works in the "Boost" state. When $|E_1|-|E_2|> \varepsilon_2$, the AC Source need provide partial power to R_2 during the positive half period of AC voltage, and the equivalent circuits of the converter are depicted in Fig. 5. It can be seen that when S_1 and S_2 are on, the AC Source supplies the power to the coupled indictor; when S_1 and S_2 are off, the power stored in the coupled inductor will be released to R_2, where the whole system works in the "Flyback" state.

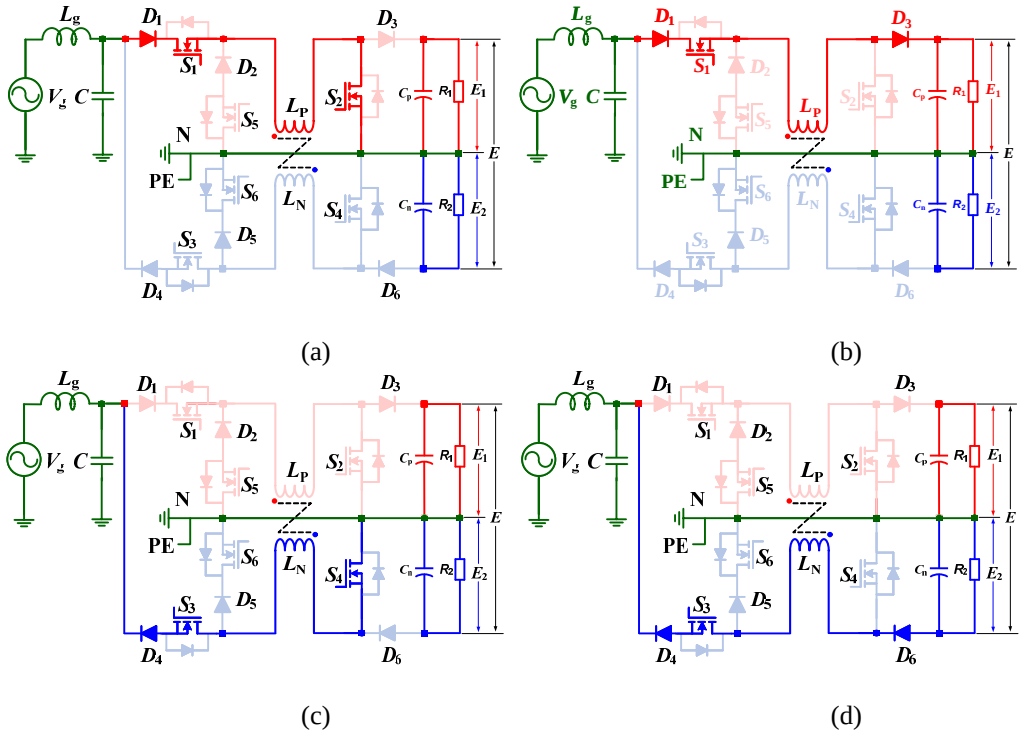

Fig. 4. Equivalent circuits in the "Boost" state: (a) Energy storing in the positive half of line period, (b) Energy releasing Energy storing in the positive half of line period, (c) Energy storing in the negative half of line period, (d) Energy releasing in the negative half of line period.

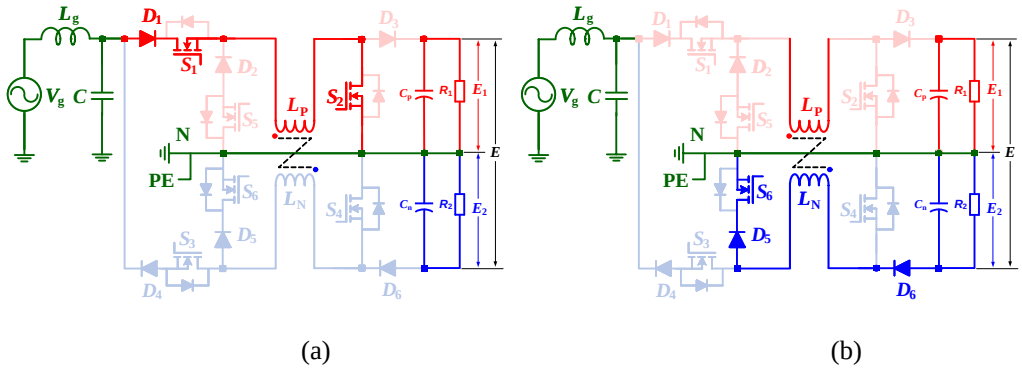

Fig. 5. Equivalent circuits in the "Flyback" state: (a) Energy storing, (b) Energy releasing.

2) $|E_1|$ and $|E_2| < V_{g\_A}$

When the output DC voltages (E_1, and E_2) are lower than the amplitude value of the grid voltage (V_{g_A}), the working sequence can be separated into six parts during a line period of AC voltage, which is similar to Fig. 2 (b).

This article has been accepted for publication in a future issue of this journal, but has not been fully edited. Content may change prior to final publication. Citation information: DOI 10.1109/TPEL.2018.2820173, IEEE Transactions on Power Electronics

When $|E_1|-|E_2| < \varepsilon_2$, the output DC voltages need not to be regulated. During T_1, T_3, T_4, and T_6, the converter works like a pure Boost converter, the equivalent circuits are just as shown in Fig. 4. During T_2 and T_5, the output DC voltages (E_1, and E_2) are smaller than the amplitude value of grid voltage V_{g_A}. During T_2, S_1 works with high frequency, S_5 is on and the rest of the switches are off. During T_5, S_3 works with high frequency, S_6 is on and the rest of the switches are off. The converter works like a pure Buck converter, where the equivalent circuits can be depicted in Fig. 6.

When $\varepsilon_1 > |E_1|-|E_2| > \varepsilon_2$, during the positive half period of the AC voltage, a partial power from the AC source will be supply towards R_2 to balance the output DC voltages. Here, a partial time of T_2 as shown in Fig. 2 (b) is served as the period of output energy regulation. Fig. 7 shows the equivalent circuits during the output energy regulation, where S_1 works at high frequency, S_6 is on, and the rest of the switches are off. When S_1 is on, the AC Source supplies the power to L_P and R_1. When S_1 is off, the power stored in coupled inductor will be released to R_2. In this scenario, the whole system works like in the "Flybuck" state.

When $|E_1|-|E_2| > \varepsilon_1$, the output DC voltages are in the serious unbalance. Then, during the output energy regulation, the system should work in the "Flyback" state as introduced in Fig. 5.

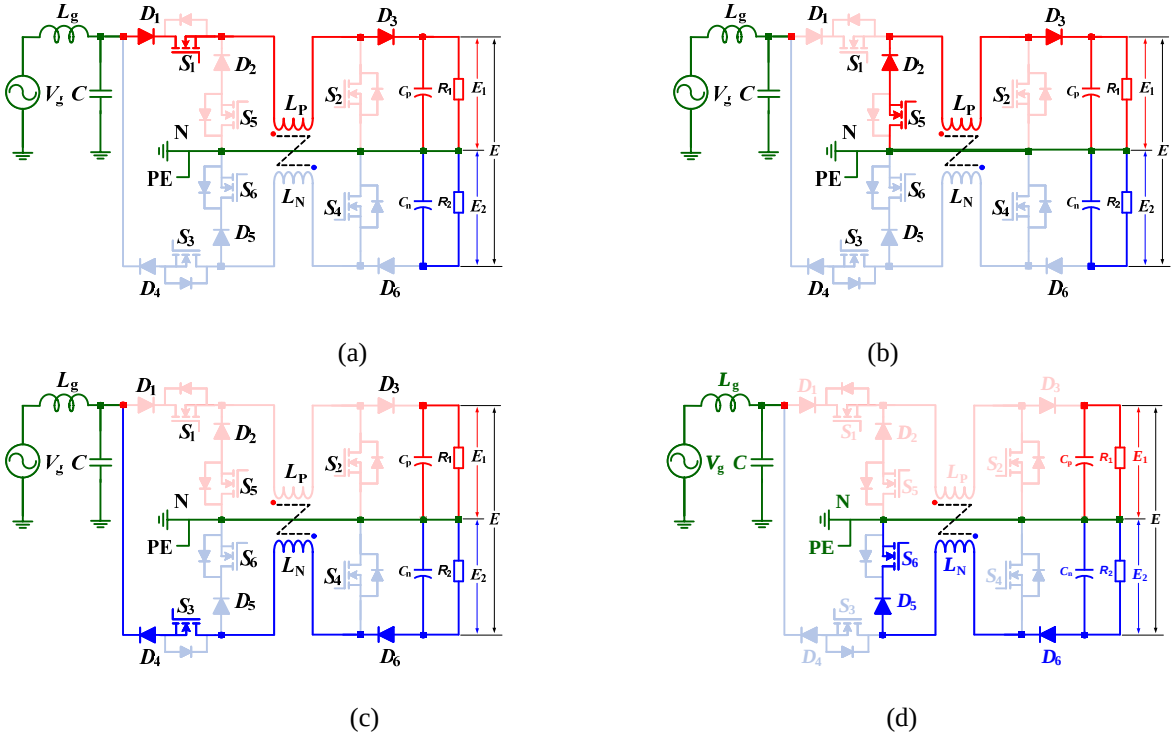

Fig. 6. Equivalent circuits in the "Buck" state: (a) Energy storing in the positive half of line period, (b) Energy releasing in the positive half of line period, (c) Energy storing in the negative half of line period, (d) Energy releasing in the negative half of line period.

This article has been accepted for publication in a future issue of this journal, but has not been fully edited. Content may change prior to final publication. Citation information: DOI 10.1109/TPEL.2018.2820173, IEEE Transactions on Power Electronics

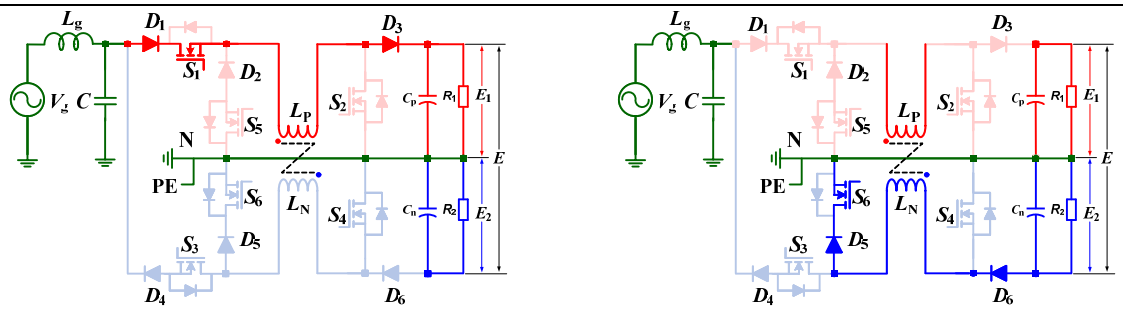

(a) (b)

Fig. 7. Equivalent circuits in the "Flybuck" state: (a) Energy storing, (b) Energy releasing.

IV. CONTROL ANALYSIS AND DESIGN

According to the analysis in section III, all the working states of proposed AC/DC converter can be summarized in Table I, when $R_1>R_2$.

Table I. Working states of the proposed AC/DC converter when $R_1>R_2$.

Working conditions	$\|E_1\|$ and $\|E_2\| > V_{g\_A}$		$\|E_1\|$ and $\|E_2\| < V_{g\_A}$			
	Positive of V_{g_A}	Negative of V_{g_A}	T_1,T_3	T_2	T_4,T_6	T_5
$\Delta < \varepsilon_2$	Boost	Boost	Boost	Buck	Boost	Buck
$\varepsilon_1 < \Delta < \varepsilon_2$	Flyback		Boost	Flybuck		
$\Delta > \varepsilon_1$			Flyback			

where $\Delta = |E_1|-|E_2|$.

From Table I, it can be seen that the working stages of proposed AC/DC converter include "Boost", "Flyback", "Buck" and "Flybuck". Using the quasi-average state small signal modeling method [35], [36] and assuming that no disturbance is coming from the DC source and the AC source, then the small signal modeling can be derived. Equation (1)-(4) are the control to grid current transfer functions of "Boost", "Flyback", "Buck" and "Flybuck" stages respectively.

$$\left.\frac{\hat{i}_{Lg}(s)}{\hat{d}(s)}\right|_{\substack{\hat{e}_1(s)=0\\ \hat{v}_g(s)=0}} = \frac{E_1 \text{ or } E_2}{s^3 L_g L_m C + s(L_g + L_m)} \tag{1}$$

$$\left.\frac{\hat{i}_{Lg}(s)}{\hat{d}(s)}\right|_{\substack{\hat{e}_1(s)=0\\ \hat{e}_2(s)=0\\ \hat{v}_g(s)=0}} = \frac{sL_m I_{LP} + D(V_C + |E_2|)}{s^3 L_g L_m C + s(D^2 L_g + L_m)} \tag{2}$$

$$\left.\frac{\hat{i}_{Lg}(s)}{\hat{d}(s)}\right|_{\substack{\hat{e}_1(s)=0\\ \hat{v}_g(s)=0}} = \frac{sL_m I_{LP} + DV_C}{s^3 L_g L_m C + s(D^2 L_g + L_m)} \tag{3}$$

$$\left.\frac{\hat{i}_{Lg}(s)}{\hat{d}(s)}\right|_{\substack{\hat{e}_1(s)=0\\ \hat{e}_2(s)=0\\ \hat{v}_g(s)=0}} = \frac{sL_m I_{LP} + D(V_C - E_1 + |E_2|)}{s^3 L_g L_m C + s(D^2 L_g + L_m)} \tag{4}$$

This article has been accepted for publication in a future issue of this journal, but has not been fully edited. Content may change prior to final publication. Citation information: DOI 10.1109/TPEL.2018.2820173, IEEE Transactions on Power Electronics

where $L_m \approx L_P = L_N$.

From the equations (1)-(4), it can be seen that the system is a typical third order system, and many papers have analyzed the control design on similar systems, especially for LCL filter or LLCL filter based grid-tied converter [37]-错误!未找到引用源。. Similar control design method is also adopted for the proposed converter. Due to the length limitation, more detailed design of the controller is not given in this paper. Fig. 8 depicts the whole control diagram of proposed AC/DC converter, where the input signals include the DC voltage of E_1 and E_2, the grid voltage of V_g (t), and the reference current i_{ref} can be obtained by using the DC voltage control loop.

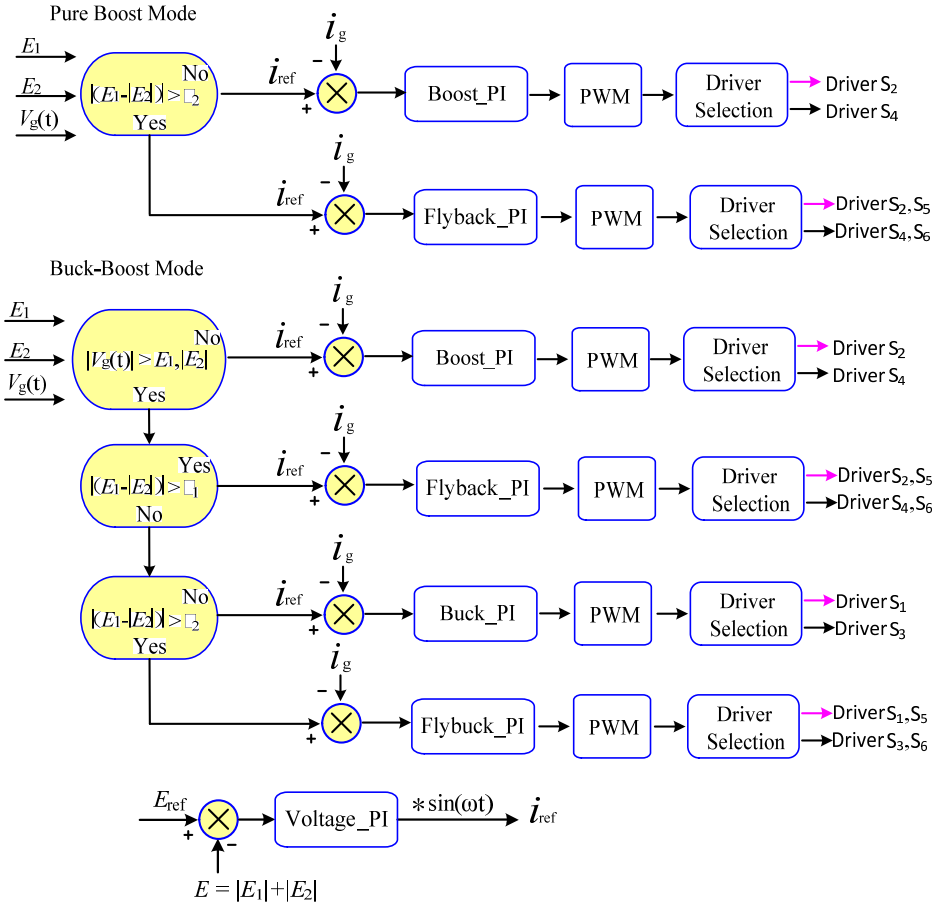

Fig. 8. Control diagram of the proposed converter.

Ⅴ. EXPERIMENTAL RESULTS

In order to verify the performance of the proposed converter, a 220 V/ 50 Hz/ 1.5 kW prototype is developed in the laboratory. The control algorithm is implemented by a digital signal processor (DSP) TMS320F2812. The type of MOSFET is IPW60R045CP, the type of diode is IDW30G65C5. A programmable AC source (Chroma 6530) is used to generate the grid voltage. The photograph of the prototype is shown in Fig. 9. The parameters of converter are listed in Table II.

This article has been accepted for publication in a future issue of this journal, but has not been fully edited. Content may change prior to final publication. Citation information: DOI 10.1109/TPEL.2018.2820173, IEEE Transactions on Power Electronics

Table II. Power converter parameters for experiments

Capacitors				Coupled inductor (L_X, X=P, N)							f_s	L_g
C_P, C_N		C										
Type	Value	Type	Value	Core material	Turns of coil	Diameter of wire	L_X	L_m	R_{LX_DC}	R_{LX_AC}		
EPCOS B43310-A5478-M	4700 μF	IKC CBB22	2 μF	PC40	26	1.6 (mm)	0.78 mH	0.7797 mH	0.1 Ω	0.2584 Ω	40 kHz	0.6 mH

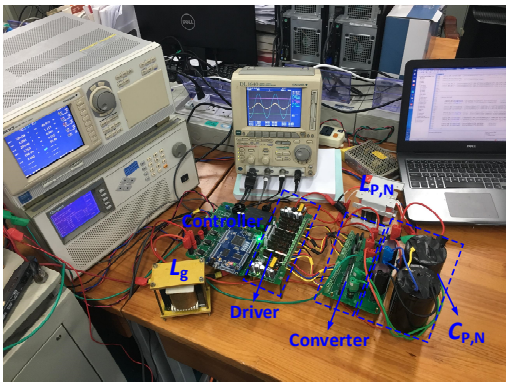

Fig. 9. Photograph of the experimental setup.

When the grid voltage is set to 110 V/50 Hz and the reference value of the DC output voltage E ($|E_1|+|E_2|$) is set to 400 V, the experimental results are shown in Figs. 10-14 respectively.

Figs. 10-11 show the gate signals of MOSFETS which work in high frequency during operation, and it can be seen that the state of switch is consistent with the principle analyzed in section III.

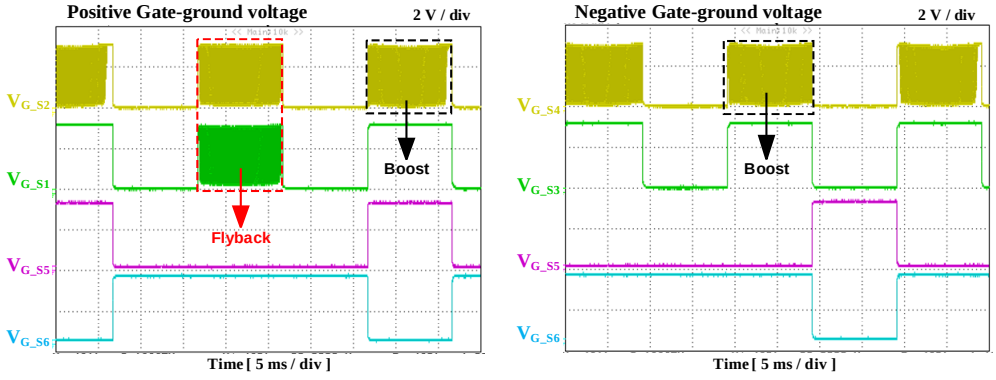

(a) (b)

Fig. 10. Mearured Gate signals of MOSFETS, when E = 400 V, and V_{gm} = 155 V: (a) During the positive operation; (b) During the negative operation.

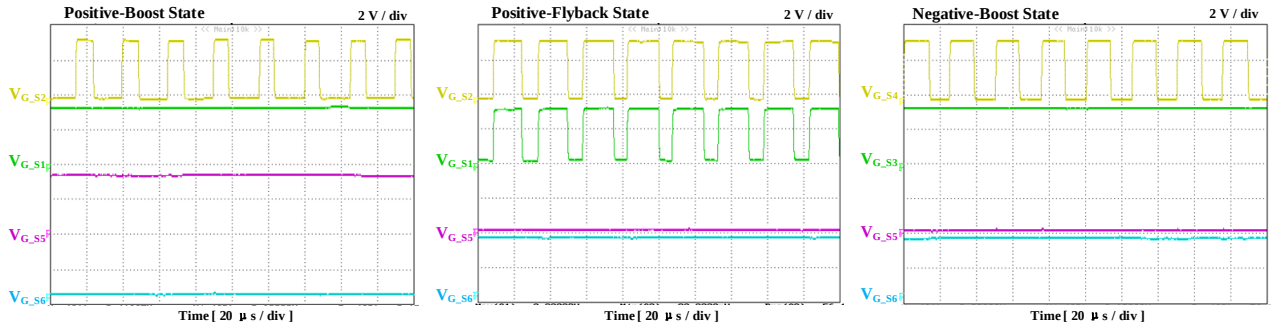

This article has been accepted for publication in a future issue of this journal, but has not been fully edited. Content may change prior to final publication. Citation information: DOI 10.1109/TPEL.2018.2820173, IEEE Transactions on Power Electronics

(a) (b) (c)

Fig. 11. Measured Gate signals of MOSFETS in different states, when E = 400 V, and V_{gm} = 155 V: (a) Positive-Boost State; (b) Positive-Flyback State; (c) Negative-Boost State.

Figs. 12 and 13 show the measured input AC voltage (V_g (t)), the output DC voltages (E_1, E_2), and the currents of inductors (i_{LN} (t), i_{LP} (t)) in the unregulated and regulated modes respectively. The grid voltage is set to 110 V / 50 Hz, and the reference value of the DC output voltage E (E_1+|E_2|) is set to 400 V.

As shown in Fig. 12, when $R_1 \neq R_2$ (R_1=144 Ω, R_2=94 Ω), it can be seen that the output DC voltage of E_1 (E_1 =223 V) is larger than the absolute value of negative output DC voltage E_2 (E_2 = -177 V), when the unregulated mode is adopted. From Fig. 13, it can be seen that for the proposed converter with coupled inductor, the output DC voltages (E_1, E_2) can be regulated to almost equal, although the loads are unbalanced. Figs. 14 shows the efficiency test results of the proposed converter in different working modes when V_g=110 V, E=400 V.

Table III shows the experimental results of the proposed converter when V_g=110 V, E=400 V. Since the flyback operation, the efficiency of the converter (η) will be reduced to 92.77%. However, the power factor (λ) and the total harmonic distortion (THD) have a little change.

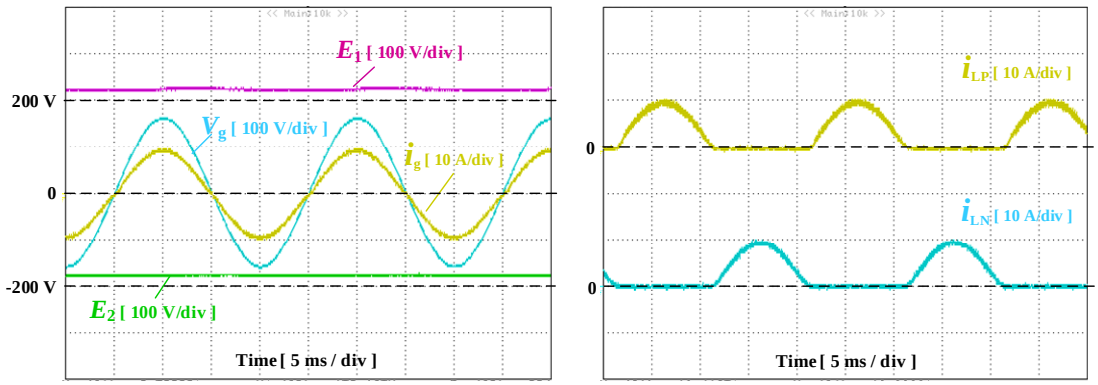

（a） (b)

Fig. 12. Measured waveforms in the unregulated mode, when E = 400 V, V_{gm} = 155 V, R_1= 144 Ω, and R_2 =94 Ω: (a) the input AC voltage (V_g (t)), and the output DC voltages (E_1, E_2); (b) the input grid current i_g and the inductor currents (i_{LP}(t), i_{LN}(t)).

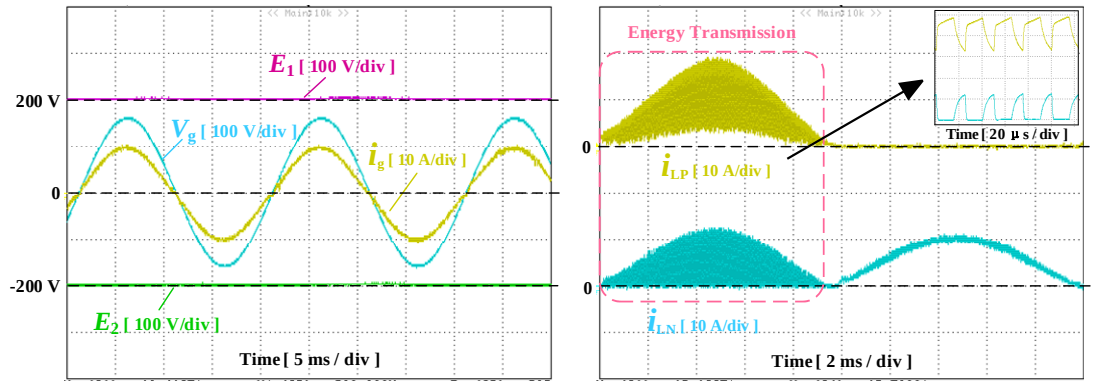

(a) (b)

This article has been accepted for publication in a future issue of this journal, but has not been fully edited. Content may change prior to final publication. Citation information: DOI 10.1109/TPEL.2018.2820173, IEEE Transactions on Power Electronics

Fig. 13. Measured waveforms in the regulated mode, when E = 400 V, V_{gm} = 155 V, R_1= 144 Ω, and R_2 =94 Ω: (a) input AC voltage (V_g(t)), and the output DC voltages (E_1, E_2); (b) the input grid current i_g, and the inductor currents (i_{LP}(t), i_{LN}(t)).

(a) (b) (c)

Fig. 14. The efficiency test results of the proposed converter when V_g=110 V, E=400 V. (a) In the balanced-load mode (R1=144Ω, R2=144Ω). (b) In the unbalanced-load mode without regulation (R1=144Ω, R2=94Ω). (c) In the unbalanced-load mode with regulation (R1=144Ω, R2=94Ω).

Table III. Experimental results of power converter when V_g=110 V, E=400 V.

Modes / Results	Balanced-load Mode R_1=144 Ω, R_2= 144Ω	Unbalanced-load Mode R_1=144Ω, R_2= 94Ω	
		Unregulated	Regulated
E_1	200.82 V	222.75 V	200.90 V
E_2	199.79 V	177.80 V	198.61 V
η	96.70%	95.28%	92.77%
λ	0.9997	0.9999	0.9999
THD	2.58%	2.68%	3.23%

When the grid voltage is set to 220 V/50 Hz, and the reference value of the DC output voltage E ($|E_1|+|E_2|$) is set to 400 V, the experimental results are shown in Figs. 15-19 respectively.

As shown in Fig. 17, when $R_1 \neq R_2$ (R_1 = 73.5 Ω, R_2 = 52 Ω), it can be seen that the output DC voltage of E_1 (E_1= 221 V) is larger than the absolute value of negative output DC voltage E_2 (E_2 = -179 V), when the unregulated mode is adopted. From Fig. 18, it can be seen that for the proposed converter with coupled inductor, the output DC voltages (E_1, E_2) can be kept almost balanced, when the loads are unbalanced.

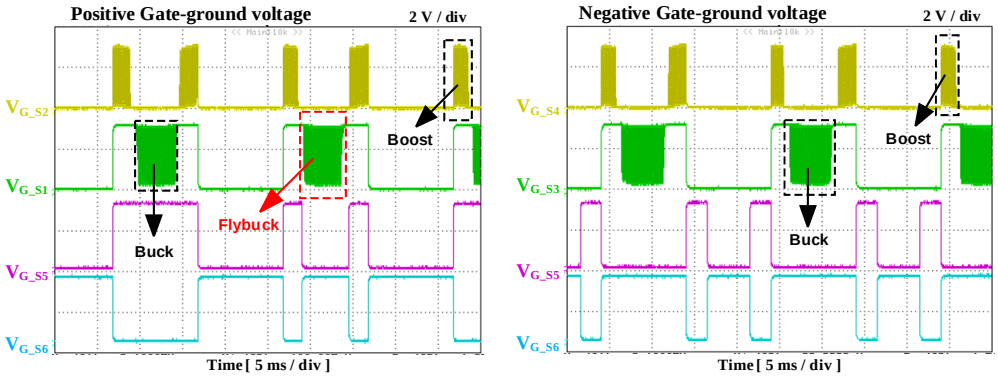

(a) (b)

This article has been accepted for publication in a future issue of this journal, but has not been fully edited. Content may change prior to final publication. Citation information: DOI 10.1109/TPEL.2018.2820173, IEEE Transactions on Power Electronics

Fig. 15. Mearured Gate signals of MOSFETS, when E = 400 V, and V_{gm} = 311 V: (a) During the positive operation; (b) During the negative operation.

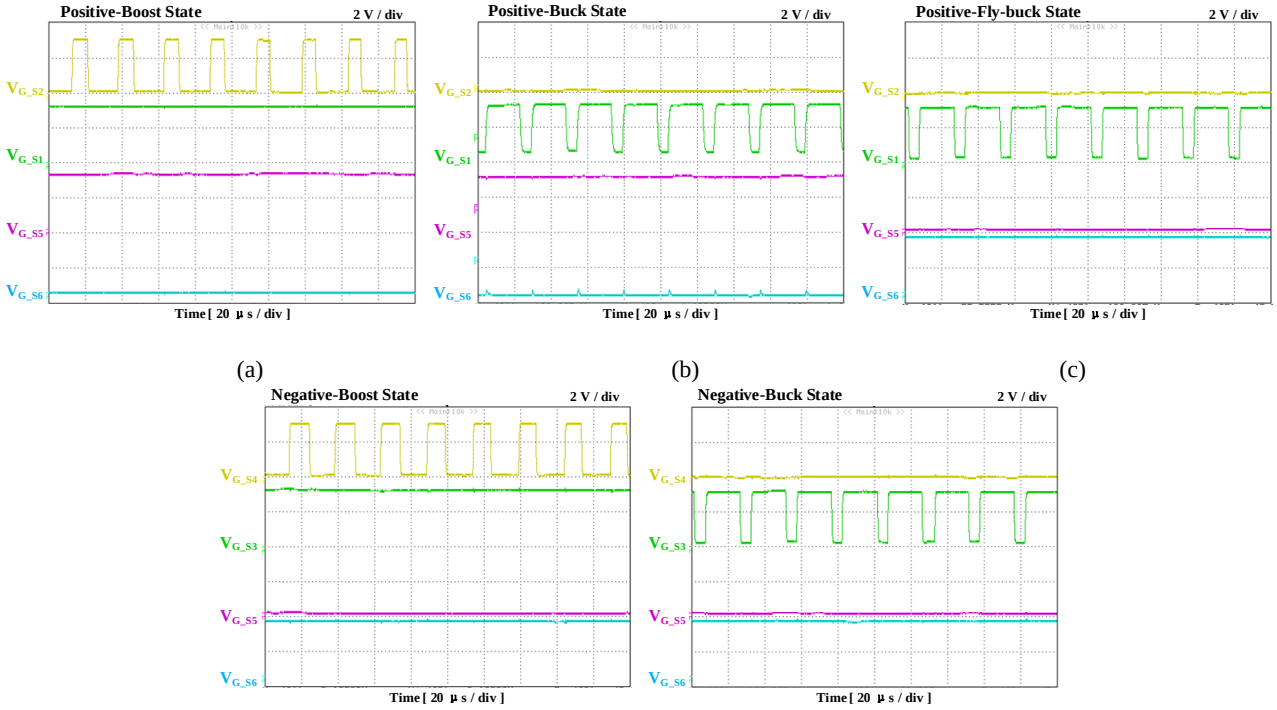

Fig. 16. Mearured Gate signals of MOSFETS in different states, when when E = 400 V, and V_{gm} = 311 V: (a) Positive-Boost State; (b) Positive-Buck State; (b) Positive-Flyback State; (c) Negative-Boost State; (c) Negative-Buck State.

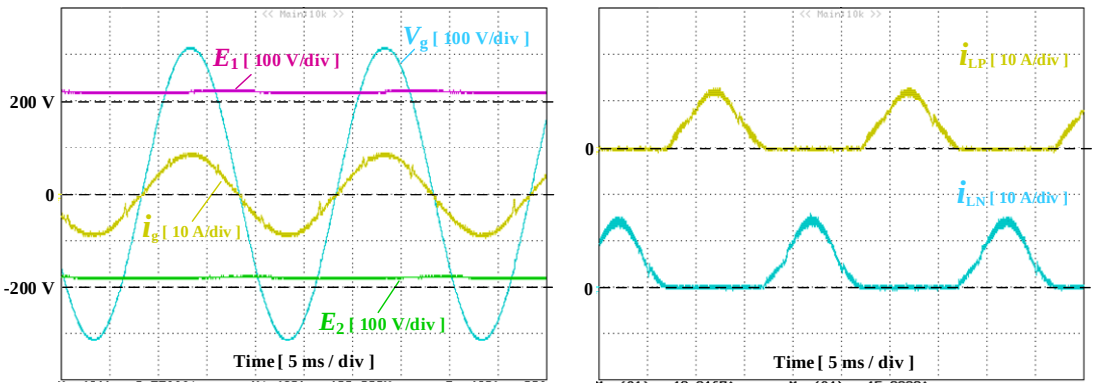

Fig. 17. Measured waveforms in the unregulated mode, when E = 400 V, V_{gm} = 311 V, R_1= 73.5 Ω, and R_2 = 52 Ω: (a) the input AC voltage (V_g (t)), the and output DC voltages (E_1, E_2); (b) the input grid current i_g, and the inductor currents (i_{LP}(t), i_{LN}(t)).

This article has been accepted for publication in a future issue of this journal, but has not been fully edited. Content may change prior to final publication. Citation information: DOI 10.1109/TPEL.2018.2820173, IEEE Transactions on Power Electronics

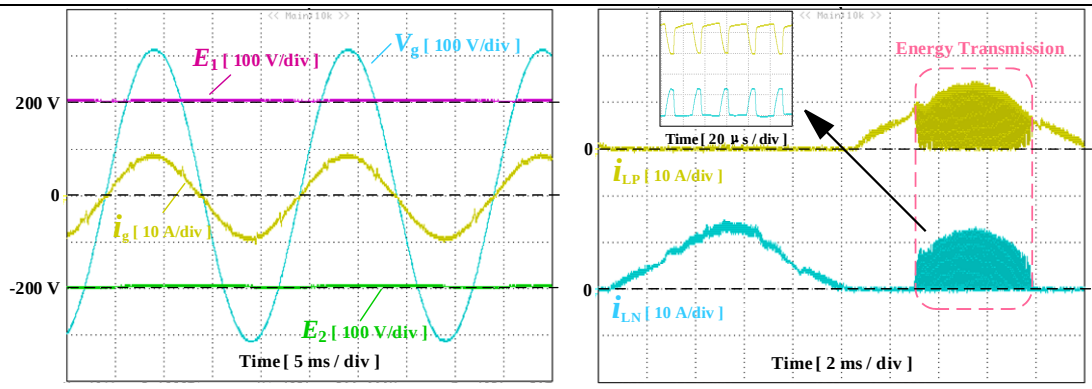

(a) (b)

Fig. 18. Measured waveforms in the regulated mode, when E = 400 V, V_{gm} = 311 V, R_1= 73.5 Ω, and R_2 = 52 Ω: (a) the input AC voltage (V_g(t)), the and output DC voltages (E_1, E_2); (b) the input grid current i_g, and the inductor currents (i_{LP}(t), i_{LN}(t)).

(a) (b) (c)

Fig. 19. The efficiency test results of the proposed converter when V_g=220 V, E=400 V. (a) In the balanced-load mode (R1=73.5Ω, R2=74Ω). (b) In the unbalanced-load mode without regulation (R1=73.5Ω, R2=52Ω). (c) In the unbalanced-load mode with regulation (R1=73.5Ω, R2=52Ω).

Table IV. Experimental results of power converter when V_g=220 V, E=400 V.

Modes / Results	Balanced Mode R_1=73.5Ω, R_2= 74Ω	Unbalanced Mode R_1=73.5Ω, R_2=52Ω	
		Unregulated	Regulated
E_1	201.54 V	221.00 V	203.12 V
E_2	198.54 V	179.37 V	196.78 V
η	97.52%	96.09%	96.07%
λ	0.9994	0.9998	0.9995
THD	4.35%	4.36%	3.39%

Before calculate the power losses of devices, some assumptions are done:

a. Ignoring the leakage inductance in the circuit layout.

b. Ignoring the input voltage ripple and fluctuation.

c. The dead-time and the delays are not considered.

d. The characters of the same type of devices are assumed to be the same and the characters are in accordance with the data provided by the manufacturers.

e. Supposing the junction temperature of devices is 80°C.

f. Supposing the core temperature of devices is 80°C.

This article has been accepted for publication in a future issue of this journal, but has not been fully edited. Content may change prior to final publication. Citation information: DOI 10.1109/TPEL.2018.2820173, IEEE Transactions on Power Electronics

When the proposed converter works in balanced-load state, the average power losses during the 0-0.5π period are the same as those during 0-2π, the average power losses of devices are calculated during the 0-0.5π period only. And the devices include: S_1, S_2, S_5, D_1, D_2, D_3, L_P, L_g.

Fig. 20 shows the calculated power losses of the devices, while P_{in} is 1.111 kW and V_g is 220 V versus the different output DC voltages in balanced-load state during the positive period of the AC voltage. It can be seen that the power losses of S_1 is larger than those of S_2 or S_5. Of all the devices, the power losses of L_P is the largest, where the ac resistance of L_P is 0.2584Ω and dc resistance of L_P is 0.1Ω.

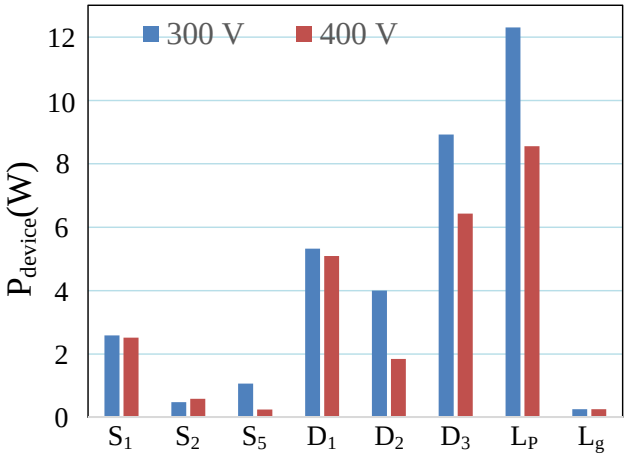

Fig. 20. Power losses distribution of devices versus the different output DC voltages (E) in balanced-load state during the positive period of the AC voltage when P_{in}=1.111 kW and V_g=220 V.

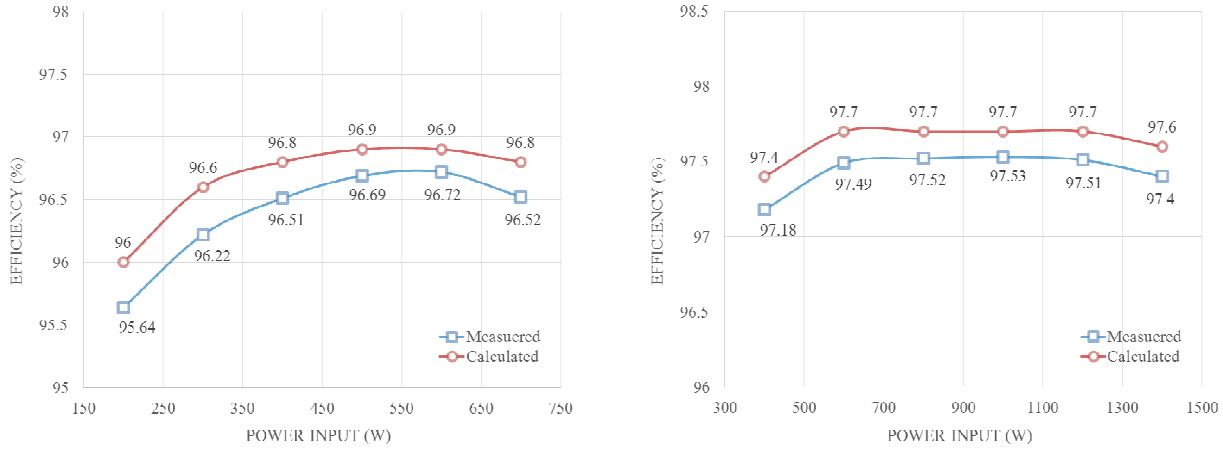

(a) (b)

Fig. 21. Calculated and measured efficiency curve of the proposed converter versus the different input power in balanced-load state (a) when E=400 V, and V_g=110 V (Pure Boost Mode), (b) when E=400 V, and V_g=220 V (Buck-Boost Mode).

Fig. 21 (a) and Fig. 21 (b) show the calculated and the measured efficiencies of the converter versus the different input power in the balanced-load state, when the input AC voltages are 110 V and 220 V respectively (not including the power losses of control circuits). It can be seen that the calculated efficiencies have similar trends as the measured efficiencies, where the measured efficiencies are lower than the calculated efficiencies, maybe due to the extra stray power losses. More

optimization design of the proposed converter needs to be carried out, for example, the design of the coupled inductor and the selection of D_3 and D_6 with the less forward voltage drop.

VI. CONCLUSIONS

In this paper, a transformerless AC/DC converter is proposed for an interface between the DC Nano-grid and the AC low voltage grid. The characteristics of this converter can be summarized as following,

1. Similar to the conventional converter presented in [26], the same ground line can be used by the AC grid and DC Nano-grid without any transformer isolation, which ensures the earth-fault protection for a hybrid power system. Note that there is still only one power stage which operates in the high frequency at any time, resulting in the high efficiency of the proposed converter.

2. Different from the conventional converter presented in [26], the new converter adopts two additional switches (S_5 and S_6) and replaces two non-coupled inductors with a single coupled inductor, where the output DC voltages can be regulated to balance, whether the loads are unequal or not.

3. The positive and the negative windings of inductor are highly coupled, where the leakage inductor can be ignored.

The principle of proposed converter has been demonstrated through the equivalent circuits. Experimental results obtained from a 220 V/ 50 Hz/ 1.5 kW prototype have verified the feasibility and effectiveness of the proposed AC/DC converter.

REFERENCES

[1] J. He, Y. W. Li, D. Xu, X. Liang, B. Liang and C. Wang, "Deadbeat Weighted Average Current Control With Corrective Feed-Forward Compensation for Microgrid Converters With Nonstandard LCL Filter," *IEEE Trans. on Power Electron.*, vol. 32, no. 4, pp. 2661-2674, April 2017.

[2] X. Guo, D. Xu, J. M. Guerrero and B. Wu, "Space Vector Modulation for DC-Link Current Ripple Reduction in Back-to-Back Current-Source Converters for Microgrid Applications," *IEEE Trans. on Ind. Electron.*, vol. 62, no. 10, pp. 6008-6013, Oct. 2015.

[3] J. He, Y. Li, C. Wang, Y. Pan, C. Zhang and X. Xing, "Hybrid Microgrid With Parallel- and Series-Connected Microconverters," *IEEE Trans. on Power Electron.*, vol. 33, no. 6, pp. 4817-4831, June 2018.

[4] J. M. Guerrero, M. Chandorkar, T. L. Lee and P. C. Loh, "Advanced Control Architectures for Intelligent Microgrids—Part I: Decentralized and Hierarchical Control," *IEEE Trans. on Ind. Electron.*, vol. 60, no. 4, pp. 1254-1262, April 2013.

[5] L. Meng et al., "Review on Control of DC Microgrids and Multiple Microgrid Clusters," *IEEE Journal of Emerging and Selected Topics in Power Electron.*, vol. 5, no. 3, pp. 928-948, Sept. 2017.

[6] X. Lu, K. Sun, J. M. Guerrero, J. C. Vasquez, L. Huang and J. Wang, "Stability Enhancement Based on Virtual Impedance for DC Microgrids With Constant Power Loads," *IEEE Trans. on Smart Grid, vol. 6*, no. 6, pp. 2770-2783, Nov. 2015.

[7] J. Rocabert, A. Luna, F. Blaabjerg and P. Rodríguez, "Control of Power Converters in AC Microgrids," *IEEE Trans. on Power Electron.*,vol. 27, no. 11, pp. 4734-4749, Nov. 2012.

[8] V. Nasirian, S. Moayedi, A. Davoudi and F. L. Lewis, "Distributed Cooperative Control of DC Microgrids," *IEEE Trans. on Power Electron.*, vol. 30, no. 4, pp. 2288-2303, April 2015.

[9] S. Anand and B. G. Fernandes, "Reduced-Order Model and Stability Analysis of Low-Voltage DC Microgrid," *IEEE Trans. on Ind. Electron.*, vol. 60, no. 11, pp. 5040-5049, Nov. 2013.

[10] J. J. Justo, F. Mwasilu, J. Lee, and J.-W. Jung, "AC-microgrids versus DC-microgrids with distributed energy resources: A review," *Renew. Sustain. Energy Rev.*, vol. 24, pp. 387–405, Aug. 2013.

[11] A. T. Elsayed, A. A. Mohamed, and O. A. Mohammed, "DC microgrids and distribution systems: An overview," *Elect. Power Syst. Res.*, vol. 119, pp. 407–417, Feb. 2015.

[12] T. F. Wu, C. H. Chang, L. C. Lin, G. R. Yu and Y. R. Chang, "DC-Bus Voltage Control With a Three-Phase Bidirectional Inverter for DC Distribution Systems," *IEEE Trans. on Power Electron.*,vol. 28, no. 4, pp. 1890-1899, April 2013.

[13] Q. Xu *et al*., "A Decentralized Dynamic Power Sharing Strategy for Hybrid Energy Storage System in Autonomous DC Microgrid," *IEEE Trans. on Ind. Electron.*,vol. 64, no. 7, pp. 5930-5941, July 2017.

[14] Y. Gu, X. Xiang, W. Li and X. He, "Mode-Adaptive Decentralized Control for Renewable DC Microgrid With Enhanced Reliability and Flexibility," *IEEE Trans. on Power Electron.*, vol. 29, no. 9, pp. 5072-5080, Sept. 2014.

[15] W. Cai, L. Jiang, B. Liu, S. Duan and C. Zou, "A Power Decoupled Method Based on Four-Switch Three-Port DC/DC/AC Converter in DC Microgrid," *IEEE Trans. on Ind. Applicat.*, vol. 51, no. 1, pp. 336-343, Jan.-Feb. 2015.

[16] P. Prabhakaran; Y. Goyal; V. Agarwal, "Novel Nonlinear Droop Control Techniques to Overcome the Load Sharing and Voltage Regulation Issues in DC Microgrid," *IEEE Trans. on Power Electron.*, vol. 33, no. 5, pp. 4477-4487, May 2018.

[17] M. H. Ryu, H. S. Kim, J. W. Baek, H. G. Kim and J. H. Jung, "Effective Test Bed of 380-V DC Distribution System Using Isolated Power Converters," *IEEE Trans. on Ind. Electron.*, vol. 62, no. 7, pp. 4525-4536, July 2015.

[18] R. Adda, O. Ray, S. K. Mishra and A. Joshi, "Synchronous-Reference-Frame-Based Control of Switched Boost Inverter for Standalone DC Nanogrid Applications," *IEEE Trans. on Power Electron.* vol. 28, no. 3, pp. 1219-1233, March 2013.

[19] S. Rivera, B. Wu, S. Kouro, V. Yaramasu and J. Wang, "Electric Vehicle Charging Station Using a Neutral Point Clamped Converter With Bipolar DC Bus," *IEEE Trans. on Ind. Electron.*, vol. 62, no. 4, pp. 1999-2009, April 2015.

[20] J. D. Park and J. Candelaria, "Fault Detection and Isolation in Low-Voltage DC-Bus Microgrid System," *IEEE Trans. on Power Deliv.*, vol. 28, no. 2, pp. 779-787, April 2013.

[21] B. Singh, B. N. Singh, A. Chandra, K. Al-Haddad, A. Pandey and D. P. Kothari, "A review of single-phase improved power quality AC-DC converters," *IEEE Trans. on Ind. Electron.*, vol. 50, no. 5, pp. 962-981, Oct. 2003.

[22] B. Singh, B. N. Singh, A. Chandra, K. Al-Haddad, A. Pandey and D. P. Kothari, "A review of three-phase improved power quality AC-DC converters," *IEEE Trans. on Ind. Electron.*, vol. 51, no. 3, pp. 641-660, June 2004.

[23] M. M. Jovanovic and Y. Jang, "State-of-the-art, single-phase, active power-factor-correction techniques for high-power applications - an overview," *IEEE Trans. on Ind. Electron.*, vol. 52, no. 3, pp. 701-708, June 2005.

[24] J. W. Kolar and T. Friedli, "The Essence of Three-Phase PFC Rectifier Systems—Part I," *IEEE Trans. on Power Electron.*, vol. 28, no. 1, pp. 176-198, Jan. 2013.

[25] T. Friedli, M. Hartmann and J. W. Kolar, "The Essence of Three-Phase PFC Rectifier Systems—Part II," *IEEE Trans. on Power Electron.*, vol. 29, no. 2, pp. 543-560, Feb. 2014.

[26] W. Wu, H. Wang, Y. Liu, M. Huang and F. Blaabjerg, "A Dual-Buck–Boost AC/DC Converter for DC Nanogrid With Three Terminal Outputs," *IEEE Trans. on Ind. Electron.*, vol. 64, no. 1, pp. 295-299, Jan. 2017.

[27] P. H. Raj, A. I. Maswood, G. H. P. Ooi and Z. Lim, "Voltage balancing technique in a space vector modulated 5-level multiple-pole multilevel diode clamped inverter," *IET Power Electron.*, vol. 8, no. 7, pp. 1263-1272, Jul. 2015.

[28] Z. Zhao, J. Zhao and C. Huang, "An Improved Capacitor Voltage-Balancing Method for Five-Level Diode-Clamped Converters With High Modulation Index and High Power Factor," *IEEE Trans. on Power Electron.*, vol. 31, no. 4, pp. 3189-3202, April 2016.

[29] V. Yaramasu, B. Wu, M. Rivera, M. Narimani, S. Kouro and J. Rodriguez, "Generalised approach for predictive control with common-mode voltage mitigation in multilevel diode-clamped converters," *IET Power Electron.*, vol. 8, no. 8, pp. 1440-1450, Aug. 2015.

[30] V. Yaramasu, B. Wu and J. Chen, "Model-Predictive Control of Grid-Tied Four-Level Diode-Clamped Inverters for High-Power Wind Energy Conversion Systems," *IEEE Trans. on Power Electron.*, vol. 29, no. 6, pp. 2861-2873, June 2014.

[31] K. Hasegawa and H. Akagi, "A New DC-Voltage-Balancing Circuit Including a Single Coupled Inductor for a Five-Level Diode-Clamped PWM Inverter," *IEEE Trans. on Ind. Appl.*, vol. 47, no. 2, pp. 841-852, March-April 2011.

[32] R. Abdullah, N. A. Rahim, S. R. Sheikh Raihan and A. Z. Ahmad, "Five-Level Diode-Clamped Inverter With Three-Level Boost Converter," *IEEE Trans. on Ind. Electron.*, vol. 61, no. 10, pp. 5155-5163, Oct. 2014.

[33] H. Wang, W. Wu, H. S. H. CHUNG and F. Blaabjerg, "Coupled-Inductor-Based Aalborg Inverter with Input DC Energy Regulation," *IEEE Trans. on Ind. Electron.*, vol. 65, no. 5, pp. 3826-3836, May 2018.

[34] Y. P. Siwakoti, F. Blaabjerg and P. C. Loh, "New Magnetically Coupled Impedance (Z-) Source Networks," *IEEE Trans. on Power Electron.*, vol. 31, no. 11, pp. 7419-7435, Nov. 2016.

[35] Z. Zhao, M. Xu, Q. Chen, J. Lai, and Y. Cho, “Derivation, analysis,and implementation of a boost–buck converter-based high-efficiency PV inverter,” *IEEE Trans. Power Electron.*, vol. 27, no. 3, pp. 1304–1313,Mar. 2012.

[36] W. Wu, J. Ji and F. Blaabjerg, "Aalborg Inverter - A New Type of “Buck in Buck, Boost in Boost” Grid-Tied Inverter," *IEEE Trans. on Power Electron.*, vol. 30, no. 9, pp. 4784-4793, Sept. 2015.

[37] W. Wu, Y. He and F. Blaabjerg, "An LLCL Power Filter for Single-Phase Grid-Tied Inverter," *IEEE Trans. on Power Electron.*, vol. 27, no. 2, pp. 782-789, Feb. 2012.

[38] Y. Liu, W. Wu, Y. He, Z. Lin, F. Blaabjerg and H. Chung, “An Efficient and Robust Hybrid Damper for *LCL*- or *LLCL*-based Grid-Tied Inverter with Strong Grid-side Harmonic Voltage Effect Rejection,” *IEEE Trans.Ind. Electron.*, vol. 63, no. 2, pp. 926-936, Feb. 2016.

[39] J. Wang, J. Yan, L. Jiang, and J. Zou, “Delay-Dependent Stability of Single-Loop Controlled Grid-Connected Inverters with *LCL* Filters,” *IEEE Trans. Power Electron.*, vol. 31, no. 1, pp. 743-757, Jan. 2016.

[40] J. Fang, X. Li, X. Yang and Y. Tang, "An Integrated Trap-LCL Filter With Reduced Current Harmonics for Grid-Connected Converters Under Weak Grid Conditions," *IEEE Trans. on Power Electronics*, vol. 32, no. 11, pp. 8446-8457, Nov. 2017.

[41] W. Wu, Y. Liu, Y. He, H. S. h. Chung, M. Liserre, F. Blaabjerg, “Damping Methods of Resonances Caused by LCL-Filter-Based Current-Controlled Grid-tied Power Inverters: an Overview”, *IEEE Trans. on Ind. Electron.*, vol. 64, no. 9, pp. 7402 - 7413, Sept. 2017.